Journal of Applied Physics ARTICLE scitation.org/journal/jap

How carbon vacancies can affect the properties of group IV color centers in diamond: A study of thermodynamics and kinetics

Cite as: J. Appl. Phys. **126**, 195103 (2019); doi: 10.1063/1.5123227
Submitted: 3 August 2019 · Accepted: 5 November 2019 ·
Published Online: 18 November 2019

Rodrick Kuate Defo,[1,a)] Efthimios Kaxiras,[1,2] and Steven L. Richardson[2,3]

AFFILIATIONS

[1]Department of Physics, Harvard University, Cambridge, Massachusetts 02138, USA
[2]John A. Paulson School of Engineering and Applied Sciences, Harvard University, Cambridge, Massachusetts 02138, USA
[3]Department of Electrical and Computer Engineering, Howard University, Washington, DC 20059, USA

[a)]**E-mail:** kuate@physics.harvard.edu

ABSTRACT

Recently, there has been much interest in using Group IV elements from the periodic table to fabricate and study XV color centers in diamond, where X = Si, Ge, Sn, or Pb and V is a carbon vacancy. These Group IV color centers have a number of interesting spin and optical properties, which could potentially make them better candidates than NV^- centers for important applications in quantum computing and quantum information processing. Unfortunately, the very same ion implantation process that is required to create these XV color centers in diamond necessarily also produces many carbon vacancies (V_C), which can form complexes with these color centers (V_C−XV) that can dramatically affect the properties of the isolated XV color centers. The main focus of this work is to use density-functional theory to study the thermodynamics and kinetics of the formation of these V_C−XV complexes and to suggest experimental ways to impede this process such as varying the Fermi level of the host diamond material through chemical doping or applying an external electrical bias. We also include a discussion of how the simple presence of many V_C can negatively impact the spin coherence times (T_2) of Group IV color centers through the presence of acoustic phonons.

I. INTRODUCTION

Solid state single photon emitters (SPEs) have become important systems in both basic and applied research because of their important applications in quantum computing, quantum metrology, and quantum information processing.[1–6] The most studied SPE to date is the negatively charged nitrogen vacancy (NV^-) in diamond, which can be made by replacing one carbon atom with a nitrogen atom, removing a neighboring carbon atom to form a vacancy, and then adding an electron to the system [see Fig. 1(a)]. The NV^- color center has an electron spin with an excellent spin coherence time (T_2) even at room temperature,[7] and this spin state can be prepared, manipulated, and read out using light and radio-frequency fields. While the spin coherence time of NV^- can be negatively affected by coupling to the ^{13}C nuclear spins in the local environment of the diamond host material,[8] the question of how a NV^- center can couple to or decouple from its neighboring nuclear spins has been studied as a means of implementing multiqubit registers.[9] Regarding the optical properties of the NV^- center, unfortunately, only about 4% of the fluorescence is found in the zero-phonon line (ZPL).[10] Another problem with using the NV^- color center as a viable SPE is that it has an electric dipole moment, thus making it susceptible to external noise and local fields, thus causing broadening in the transition level inhomogeneities. One way to solve this problem is to consider solid state SPEs, which have inversion symmetry and therefore lack a dipole moment, making them insensitive to external fields.

In a quest to identify a suitable solid state SPE with inversion symmetry, there has been a considerable amount of both experimental and theoretical work in the literature on SiV color centers.[11–32] The SiV centers in diamond can be formed by removing two adjacent carbon atoms along the ⟨111⟩ lattice direction and inserting an interstitial Si atom midway along this direction between the two vacant sites [see Fig. 1(b) where X = Si]. While

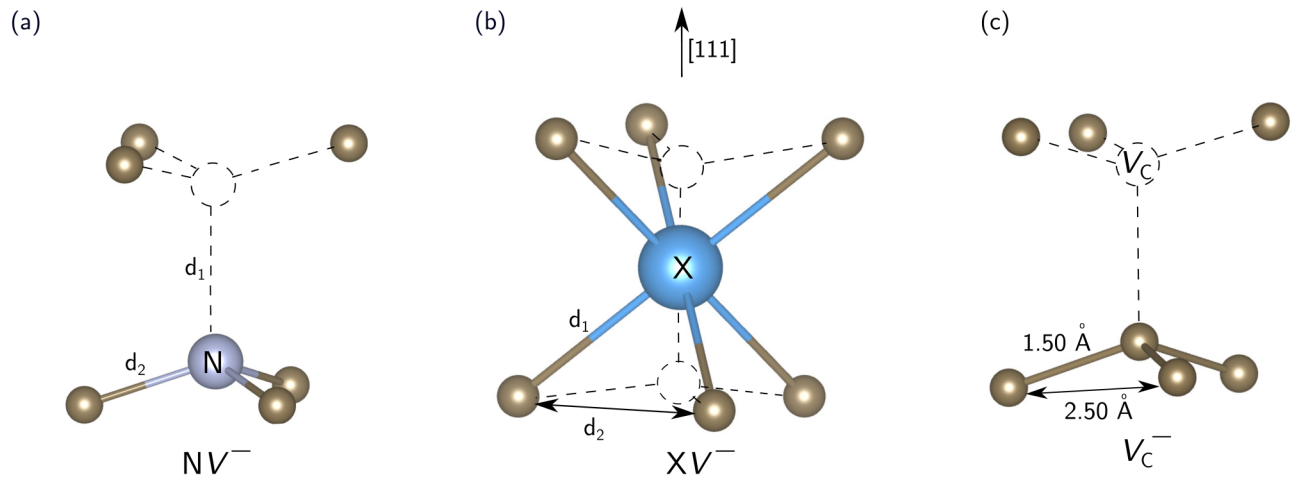

FIG. 1. Structure of (a) NV^-, (b) XV^-, and (c) V_C^- defects, with the same orientation, with distances defined corresponding to the values in Table I. Carbon atoms are indicated in brown.

the fluorescence of the charge state SiV^- color center is quite an improvement from the NV^-, with 60% of its luminescence now seen in the ZPL, it has a much shorter spin coherence time than the NV^-. It has been demonstrated that by applying strain on the SiV^-, one can enhance its spin coherence time.[33] The neutral charge state color center SiV^0 has also been extensively studied since it is expected to have an intrinsically longer spin coherence time than the SiV^-.[28,31]

One can explore other color centers beyond SiV and its various charge states by considering the general class of XV color centers, where X is a Group IV element (X = Ge, Sn, or Pb) and V is a carbon vacancy in the diamond structure. Group IV color centers are particularly interesting choices for solid state SPEs because the selection of heavier elements for X results in a larger energy split in the ground state for the singly negatively charged color center, which will increase their spin coherence time even at higher temperatures.[34] These XV color centers would also possess inversion symmetry and thus potentially be better candidates for SPEs than the NV^- in diamond. Recently, a new Group IV color center in diamond, the GeV^-, has been produced by ion implantation and chemical vapor deposition techniques[35] and also by using a microwave plasma chemical reactor.[36] The GeV^- color center has a structure very similar to SiV^-, and it has a sharp and strong ZPL at 602 nm at room temperature. Subsequent experiments have spectroscopically confirmed that GeV^- is a promising candidate for a SPE.[37–43] The SnV^- color center has been created and identified at room temperature, and it has a geometry similar to GeV^- and a photoluminescence spectrum that shows a sharp ZPL at 619 nm.[34,44] SnV^- centers have also been created under high pressure[45,46] and can be used in luminescent thermometry.[47] As demonstrated for NV^- centers, it is possible to structurally confine SnV^- color centers to reside within diamond nanopillars and thus enhance their optical properties.[48] Finally, the PbV^- color center has been fabricated and characterized as a SPE with a structure similar to that of the SiV^-, GeV^-, and SnV^- centers, though there is disagreement in the literature as to the value of its ZPL with measured values of 520 nm[49] or over 550 nm[50] and a predicted value of 517 nm.[49,51]

TABLE I. Structural constants d_1 and d_2 (in angstroms; see Fig. 1) for XV^- centers and corresponding values from previous work in parentheses.

XV	d_1	d_2
NV	1.80 (1.87[a])	1.48 (1.42[a])
SiV	1.98 (1.96[b])	2.69 (2.67[b])
GeV	2.03 (2.01[b])	2.76 (2.73[b])
SnV	2.10 (2.08[b])	2.86 (2.83[b])
PbV	2.15 (2.12[b])	2.92 (2.88[b])

[a]From Ref. 2.
[b]From Ref. 51.

In this paper, we will explore how a single carbon vacancy (V_C) can affect the properties of XV color centers in diamond. Let us first, however, review how single carbon vacancies can affect NV^- color centers in diamond. Indeed, to generate these NV^- centers, atomic and molecular nitrogen ions (e.g., $^{15}N^+$ and $^{15}N_2^+$) are introduced at low to high energies (2 keV–2 MeV) in a host diamond material where they substitutionally replace carbon atoms.[52–58] This process produces a large number of single carbon vacancies throughout the crystal especially along the pathway of the implanted nitrogen ions. Subsequent annealing of the host diamond material at high temperature eliminates many of these newly created carbon vacancies, while others can diffuse toward the implanted nitrogen atoms to form the desired NV^- color centers. Unfortunately, the remaining single carbon vacancies in the host material can cause several problems for these newly created NV^- color centers. One issue is that a V_C can form a complex with a NV^- color center (e.g., V_C–NV^-), thus affecting its optical properties by quenching its fluorescence (the more prevalent an issue

becomes, the heavier the color center).[56] Another problem occurs when single carbon vacancies combine to form paramagnetic clusters of various shapes and sizes $(V_C)_{n=2,3,...}$, which can interfere with the spin of the NV^- centers, thus decreasing their spin coherence times.[59–61] A clever way of eliminating the formation of vacancy clusters when creating NV^- centers in diamond has been recently proposed.[62] By charging the vacancies in the space charge layer of free carriers generated by a boron-doped diamond structure, the formation of thermally stable paramagnetic divacancy complexes (V_2) was suppressed, resulting in a tenfold-improved spin coherence time for the color centers and a twofold-improved formation yield of nitrogen vacancy centers in diamond. We believe that all of these concerns would also apply for the carbon vacancies, which were generated during the formation of XV color centers.

As a first step in understanding how carbon vacancy clusters can affect the properties of XV color centers in diamond, we consider in this paper the simplest example of a carbon vacancy cluster, the single isolated V_C in diamond, and study the thermodynamics of the formation of a V_C–XV complex using density-functional theory (DFT). We compute the diffusion barrier height of an isolated V_C in diamond and study how it is altered in the presence of a nearby XV color center. As motivated by the work on carbon vacancy clusters on the NV^- center,[62] we then model the formation of the V_C–XV complex as a function of its charge state and the Fermi level of the host diamond material. These results might propose ways to mitigate the formation of V_C–XV clusters by simple electromagnetic and chemical considerations under certain doping conditions. Finally, we address the problem that while acoustic phonons can have a detrimental effect on the spin coherence times of XV color centers, and the NV^- color center as well, this effect can be mitigated by varying the density of carbon vacancies in the host diamond material.

In this paper, we first review and discuss methods we will use in our computations (Sec. II). In Sec. III, we use DFT to compute the optimized geometries (Sec. III A) and formation energies and charge transition levels (Sec. III B) for the isolated V_C, the NV defect, and the XV defects as well, where X is a Group IV element (X = Si, Ge, Sn, or Pb). Our calculated results in Sec. III are also compared with available experimental and theoretical results. In Sec. III C, we compute the lowest energy diffusion pathway for an isolated V_C, determine its diffusion barrier height, and demonstrate that it is a function of the charge state of V_C and thus the Fermi level of the host material. In an effort to evaluate the ease with which the V_C–XV complex can form kinetically, in Sec. III D, we then study the effect of a neighboring XV color center on the diffusion barrier height of a V_C as a function of the charge state of the V_C and the Fermi level of the host material. Since we show in this paper that the formation energies for the isolated V_C and the isolated XV color center depend on both their individual defect charge states and the Fermi level of the host material, we develop in Sec. III E a detailed model, which will enable us to compute the formation energy of a V_C–XV complex while ensuring charge conservation for the system. In Sec. III F, we propose a model to explore the effect of carbon vacancies on the acoustic phonons of the host diamond material and how this could affect the spin coherence time of XV color centers and then summarize the conclusions of this work.

II. COMPUTATIONAL METHODS

We performed first-principles DFT calculations for the various defect structures using the VASP code.[63–65] For the exchange-correlation energy of electrons, we use the generalized gradient approximation (GGA), as parametrized by Perdew, Burke, and Erzenhof (PBE).[66] The atomic positions were relaxed until the magnitude of the Hellmann-Feynman forces was smaller than 0.01 eV Å^{-1} on each atom, and the lattice parameters were concurrently relaxed. The wavefunctions were expanded in a plane wave basis with a cutoff energy of 600 eV, and a Monkhorst-Pack grid of $18 \times 18 \times 18$ k-points was used for integrations in the reciprocal space for the stoichiometric conventional unit cell. The relaxed lattice parameters of the stoichiometric conventional unit cell were then used for all other structures. As a test of the level of convergence of energies and structural features, we checked that the increase in the grid size from $12 \times 12 \times 12$ to $18 \times 18 \times 18$ and in the cutoff size from 400 eV to 600 eV caused a change in the total energy of less than 0.02 eV and a change in the lattice constants of less than 0.01 Å. Formation energies and transition states were calculated using a supercell with 216 atoms ($3 \times 3 \times 3$ multiple of the conventional unit cell) with appropriately scaled k-point grids and a cutoff energy of 400 eV. Supercells that were a $4 \times 4 \times 4$ multiple of the conventional unit cell were also investigated to check the convergence of the results.

The formation energies of $XV^{(q)}$ (X = N, Si, Ge, Sn, Pb) in various charge states were calculated according to the formula,[67,68]

$$E_f(q) = E_{\mathrm{def}}(q) - E_0 - \sum_i \mu_i n_i + q(E_{\mathrm{VBM}} + E_{\mathrm{F}}) + E_{\mathrm{corr}}(q), \quad (1)$$

where q denotes the charge state, with $q \in [-3, +2]$, $E_{\mathrm{def}}(q)$ is the total energy for the defect supercell with the charge state q, E_0 is the total energy for the stoichiometric neutral supercell, μ_i is the chemical potential of atom i, n_i is a positive (negative) integer representing the number of atoms added (removed) from the system relative to the stoichiometric cell, E_{VBM} is the absolute position of the valence band maximum, E_{F} is the position of the Fermi level with respect to the valence band maximum (generally treated as a parameter), and $E_{\mathrm{corr}}(q)$ is a correction term to account for the finite size of the supercell when performing calculations for charged defects.[69] This correction term does not simply treat the charged defect as a point charge but rather considers the extended charge distribution. The chemical potentials of all the reference elements used in our calculations are listed as follows as a function of their crystal structure and total energy per atom: N (β hexagonal close-packed structure, −8.29 eV/atom); C (diamond structure, −9.10 eV/atom); Si (diamond structure, −5.42 eV/atom); Ge (diamond structure, −4.49 eV/atom); Sn (body-centered tetragonal structure, −3.80 eV/atom); and Pb (face-centered cubic structure, −3.57 eV/atom). For diffusion studies, all defect atoms were located at the same position in the crystal lattice relative to the V_C with the exception of N, which was considered at two positions such that its average position in the crystal lattice relative to the V_C was the same as that of the other defect atoms.

For calculating the barriers for diffusion, we used the nudged elastic band (NEB) method.[70,71] The atomic positions were first

relaxed in the initial and final $3 \times 3 \times 3$ supercell configurations until the threshold of $0.01\,\text{eV}\,\text{Å}^{-1}$ was reached. Three images between the endpoints were then constructed by linearly interpolating between the endpoints, and each image was relaxed to the force threshold of less than $0.01\,\text{eV}\,\text{Å}^{-1}$ on each atom. A spring force was set up between neighboring images such that the relaxation would occur predominantly in the direction perpendicular to the hypertangent between images, thus ensuring the preservation of equal distances between images.

To fully characterize diffusion, the diffusivity, D, is given by

$$D = \nu_0 d^2 e^{-\varepsilon_b/k_B T}, \tag{2}$$

where $\nu_0 = \nu_0(T)$ is the attempt frequency, d is the migration distance, in the case of V_C equal to the nearest neighbor hop between C sites, and ε_b is the activation energy barrier. From harmonic transition-state theory, we calculate the attempt frequency as[72]

$$\nu_0 = \frac{k_B T}{h} \prod_{j=1}^{m'} \frac{e^{-h\nu_j'/2k_B T}}{(1 - e^{-h\nu_j'/k_B T})} \left(\prod_{j=1}^{m} \frac{e^{-h\nu_j/2k_B T}}{(1 - e^{-h\nu_j/k_B T})} \right)^{-1}, \tag{3}$$

where m, m' and ν_j, ν_j' are the corresponding number of normal modes and phonon frequencies, respectively, at the initial (I) and saddle-point (S) configurations (there is one fewer normal mode at the saddle point than at the equilibrium configuration, $m = m' + 1$).

The charge at the V_C was obtained using the DDEC6 method.[73] These density derived electrostatic and chemical (DDEC) methods for calculating the charge assign to each atom a charge density. Such charge densities are optimized with respect to distance functions designed to respect ionic and covalent bonding and with the constraint that the sum of the atomic charge densities equals the total charge density.[74] The DDEC6 method is preferable to Bader's quantum chemical topology (QCT), which can lead to non-nuclear attractors and thereby undefined net atomic charges (NACs).[75] The DDEC6 method is an improvement from the DDEC3 approach, which does not always converge to a unique solution or one that respects the symmetries of the system.[73] Finally, the DDEC6 method is also preferable to such methods as the Mulliken population analysis, which is not independent of the chosen basis.[76]

As input to our first-principles phonon calculations, which were performed using Phonopy,[77] a supercell was constructed containing 64 atoms ($2 \times 2 \times 2$ multiple of the conventional unit cell) with appropriately scaled k-point grids and a cutoff energy of 500 eV. In constructing the input supercells with defects for Phonopy, the atomic positions were relaxed until the magnitude of the Hellmann-Feynman forces was smaller than $10^{-4}\,\text{eV}\,\text{Å}^{-1}$.

III. RESULTS AND DISCUSSION

A. Optimized geometries

For the structural features of diamond, we obtain $a = 3.572$ Å for the lattice constant. Our value agrees well with the experimental value of $a = 3.567$ Å[78] and with a theoretical value of $a = 3.570$ Å.[2] Various structural constants are defined in Fig. 1, and the values for the different color centers are presented in Table I, as obtained from our calculations and from previous theoretical investigations.[2,51]

B. Formation energies

In order to relate the barrier height as a function of charge of V_C to the Fermi level, we computed formation energies and charge transition levels for the defects, which are shown in Fig. 2(a). Formation energies for a representative case, the NV defect, are shown in Fig. 2(b). Our results for the formation energy of the NV defect in diamond are in good agreement with previous results,[2]

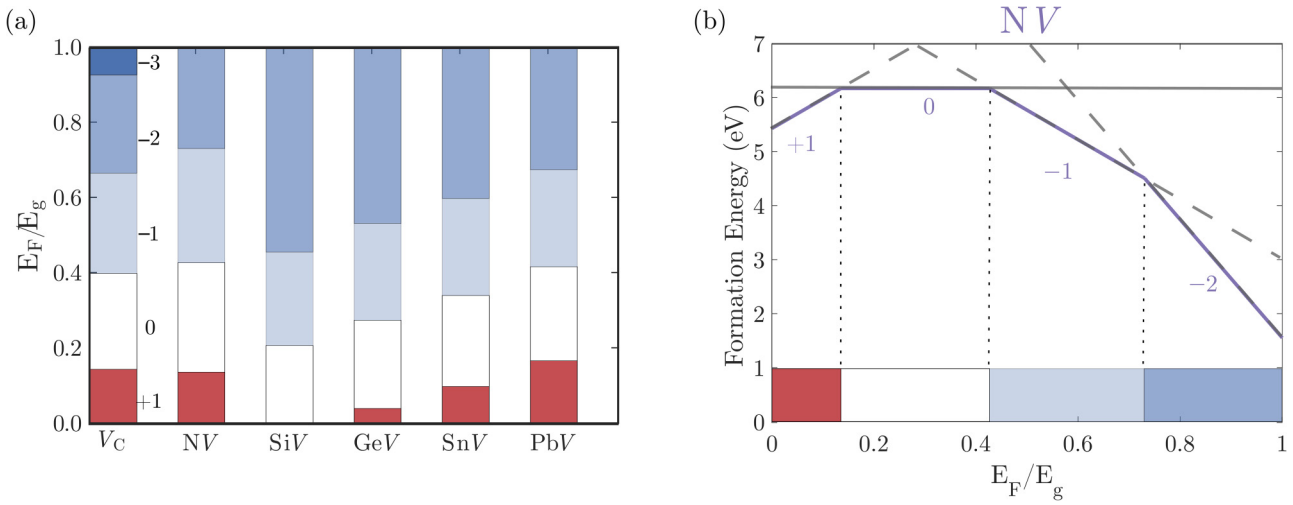

FIG. 2. (a) Charge transition levels shown relative to the experimental gap $E_g = 5.47$ eV,[79] for the unit cell with 216 atoms for V_C, NV, SiV, GeV, SnV, and PbV. The calculated gap was $E_g^{DFT} = 4.10$ eV. (b) Sample formation energy plot for the NV defect, from which charge transition levels are obtained.

and our results agree with the charge state of GeV found experimentally for intrinsic diamond.[41]

Our formation energy for the neutral V_C, shown in Fig. 3, of 7.00 eV is in good agreement with values from the literature of 6.74 eV and 6.86 eV, using a 128-atom supercell with the B3LYP functional and using a 456-atom hydrogen-terminated cluster through the CRYSTAL code, respectively,[80] or 7.01 eV and 6.99 eV using 32- and 64-atom supercells, respectively, with the HSE06 functional[81] or 6.78 eV using Vanderbilt ultrasoft pseudopotentials with a 64-atom supercell.[82] We note that the calculated formation energies for the V_C are consistent with the experimental observations of the dependence of the GR1 color center (which has been assigned to the neutral defect) on the Fermi level in diamond.[83] We also note that our transition levels for the SiV are in good agreement with Ref. 14 where the charge correction scheme of Lany and Zunger was used[84] as well as the HSE06 functional with a 512-atom supercell. Given the lower order of approximation possible with the PBE functional, we miss the +1 charge state as our transition levels are shifted slightly. Using the Kröger-Vink notation to describe a transition level,[68,85] the $(-|0)$ level is at a reduced Fermi level of 0.21 compared to 0.26,[14] and the $(2-|-)$ level is at a reduced Fermi level of 0.45 compared to 0.39.[14] Thus, we assign an error to our transition levels of roughly 6% of E_g.

C. Diffusivity of isolated V_C in diamond

We now turn to the formation of complexes of the V_C with XV color centers in diamond. The first step in our model calculation is to compute the barrier height of diffusion for an isolated V_C in diamond as a function of the charge state of the vacancy q. We used the NEB method to compute the lowest energy diffusion pathway for an isolated V_C in diamond and then calculated the barrier height ($E_b^{V_C}$) for that particular lowest energy pathway. We then hypothesized that this barrier height would also depend upon the charge state of the isolated V_C. To test our hypothesis, we performed a model calculation in which we computed the barrier height for diffusion of the V_C as a function of the charge state of the vacancy, q. It is important to realize that in our actual DFT calculation, we cannot directly alter the charge state of the V_C in diamond. We can, however, modulate the total charge of the supercell, which contains the isolated V_C, and this total charge is redistributed throughout the supercell as a result of the DFT calculation. We used the DDEC6 method (see Sec. II) to compute the charge state of the V_C for a particular choice of the total charge of the supercell, which contains the isolated V_C (we chose nine different values for the total charge of the system from $-6e$ to $+2e$). We note that our barriers for the neutral isolated V_C and the isolated V_C^- of about 2.6 eV and 3 eV, respectively, are in good agreement with other theoretical values of 2.6 eV and 3.5 eV.[2] Our results for the barrier height for an isolated V_C in diamond as a function of its charge state q are illustrated in Fig. 4.

The V-shaped behavior of the barrier as a function of charge can be interpreted to first-order using very simple chemical and physical ideas. Starting at the right-hand side of Fig. 4 and moving toward the left corresponds to increasing the Fermi level of the host material. From a practical point of view, this can be accomplished by doping diamond with electrons, thus making more electrons available in the conduction band. These excess electrons are now available to the V_C and stabilize the dangling bonds surrounding it. This results in a lower barrier height since the presence of the passivating charge reduces the energy required to break and reform chemical bonds during the diffusion of V_C throughout the diamond host material. As the Fermi level is increased further, a point is reached where the V_C becomes saturated with charge, and it can no longer acquire more electrons to passivate the neighboring dangling bonds. The excess charge interacts with the charge around

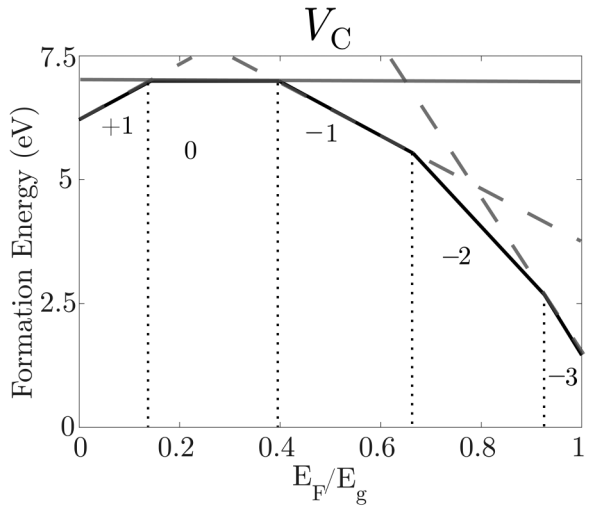

FIG. 3. Formation energy for the most stable charge state of the V_C as a function of the normalized Fermi level. Vertical dotted lines indicate transitions between charge states.

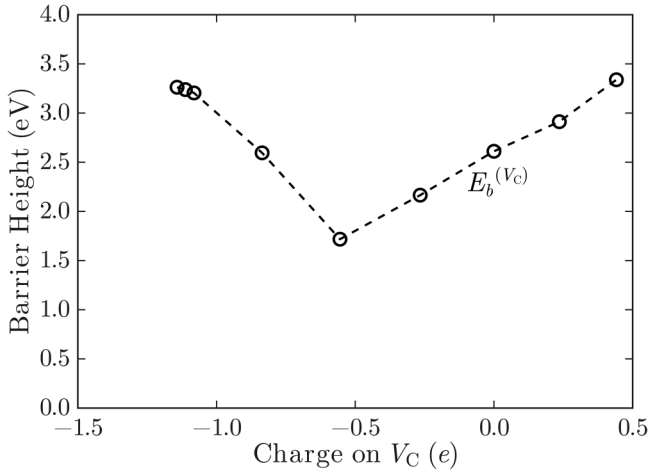

FIG. 4. Charge dependence of the barrier $E_b^{(V_C)}$ for diffusion for the isolated V_C (black open circles) in diamond. The lines between data points are a guide to the eye.

the V_C, and the ensuing Coulomb repulsion causes an increase in the diffusion barrier height. In summary, our model calculation shows that the charge of the V_C must be taken into account to determine how easy or hard it is for the defect to diffuse. This barrier height is implicitly a function of the Fermi level of the host semiconductor material since the expected charge state depends on the Fermi level position, which can be altered either by doping or through the application of an external bias.

In the high-temperature limit, we obtain an attempt frequency $\nu_0 = 6.4 \times 10^{13}\,\mathrm{s}^{-1}$ for the neutral vacancy and a higher value of $\nu_0 = 16.2 \times 10^{13}\,\mathrm{s}^{-1}$ near a DDEC6 charge of $-1e$ for the vacancy, as expected from consideration of phonons traveling through an ionized medium.[86] At 1200 °C, using $d = 1.6$ Å, we find a diffusivity of $2.4 \times 10^{-15}\,\mathrm{m}^2\,\mathrm{s}^{-1}$ for the neutral state using a barrier of 2.6 eV, corresponding to a diffusion length of $49\,\mathrm{nm\,s}^{-1}$, and a diffusivity of $2.6 \times 10^{-16}\,\mathrm{m}^2\,\mathrm{s}^{-1}$ for the -1 charge state using a barrier of 3.0 eV, corresponding to a diffusion length of $16\,\mathrm{nm\,s}^{-1}$. Thus, diffusion is important in these systems for high temperature annealing.

D. Diffusivity of V_C in the presence of XV color centers in diamond

We next investigate the ease of diffusion of V_C if it is placed near a XV color center. To address this question, we used a simple model in which both the V_C and the XV color center are placed in a $3 \times 3 \times 3$ supercell in such a manner as to maximize the distance between them by taking into account the periodicity of the supercell. Once this distance is determined, we calculated the barrier height of diffusion for the V_C in the presence of the stationary XV color center ($E_b^{(XV)}$). As previously discussed in Sec. III C for the isolated V_C, we expect this barrier height to depend on the charge state. The total charge in the supercell containing both the XV and the V_C was varied from $-6e$ to $+1e$, and these results are shown in Fig. 5.

The barrier height for V_C in the presence of XV as a function of the charge state of the V_C also has a characteristic V-shaped behavior, which is similar to that of the isolated V_C for the reasons previously discussed, but it is always higher than that of the isolated V_C. This can be explained by the fact that the XV acts as a dopant, more precisely an as acceptor, and it removes charge from the local environment of the V_C, thus making it harder to passivate the dangling bonds surrounding the V_C as it diffuses. The net effect is that the diffusion barrier height for the V_C is increased in the presence of the XV.

The results of Fig. 5 appear to suggest that carbon vacancies should tend to get stuck as they attempt to approach the XV, as a higher barrier for diffusion at a given location implies that it is harder to move away from that given location, and more so as the charge becomes more positive. In Sec. III E, we provide calculations of the thermodynamics of the relevant systems, which outline how isolation of color centers is favored under certain conditions.

We have considered the effect of increasing the size of the supercell from a $3 \times 3 \times 3$ multiple to a $4 \times 4 \times 4$ multiple of the conventional unit cell, which corresponds to an increase in the distance between defect species from 7.62 Å to 9.18 Å (a change of about 20%). These larger supercells did not produce any qualitative changes in the observed trends. The results nonetheless warrant some further discussion as for the case of the $4 \times 4 \times 4$ supercells, where the different defect species were placed slightly farther away from each other (and from their periodic images as well), we found significantly higher barriers to diffusion for the cases with a nonzero total charge than in the $3 \times 3 \times 3$ case. We explain this effect by noting that as defects approach one another, their orbitals hybridize, thus resulting in lower energies. Having explored the limiting cases of the infinite distance between the species (the isolated case) and the minimal distance between the species (discussed below) and two intermediate cases, we can conclude that the barrier for diffusion of the V_C depends on distance in the following manner: It increases from roughly zero as the distance between the species is increased until it reaches a maximum when the species are at the minimum distance where they no longer experience hybridization of orbitals and then decreases until the barrier reaches the value for the isolated V_C.

E. Thermodynamics of forming complexes of XV and V_C

We now determine the result of the reaction once a V_C in diamond reaches a color center (or is a small, but finite, distance away from one) since, as our calculations show, the V_C defects are quite mobile and can diffuse easily throughout the crystal. Based on the respective formation energies from our calculations, a V_C in close proximity to a color center is quite stable as compared to the case when the two constituents are isolated (a sample complex is shown for one of the heavier color centers, the GeV, in Fig. 6).

To understand whether, for example, a V_C−GeV complex will spontaneously form if the GeV and V_C species are brought very close together in the crystal, we compare the formation energy of the V_C-GeV complex with the formation energy of a system consisting of the two isolated V_C and GeV species for the reaction

$$V_C + \mathrm{Ge}V \rightarrow V_C - \mathrm{Ge}V. \tag{4}$$

Thermodynamically, if the formation energy of the system consisting of the two isolated species is higher than that of the complex, it follows that the complex should form spontaneously. Thus, the quantity of interest is ΔE_f for the V_C-GeV complex relative to the isolated GeV and V_C species,

$$\Delta E_f = E_f^{V_C-\mathrm{Ge}V} - E_f^{V_C} - E_f^{\mathrm{Ge}V}, \tag{5}$$

where $E_f^{V_C-\mathrm{Ge}V}$, $E_f^{V_C}$, and $E_f^{\mathrm{Ge}V}$ are the formation energies of the respective species indicated by the superscripts. The calculation of this difference is complicated by the fact that the formation energies on the right side of Eq. (5) also depend on the charge states for the individual species. Specifically,

$$E_f^{V_C} = E_f^{V_C}(q_{V_C}), \tag{6}$$

$$E_f^{\mathrm{Ge}V} = E_f^{\mathrm{Ge}V}(q_{\mathrm{Ge}V}), \tag{7}$$

$$E_f^{V_C-\mathrm{Ge}V} = E_f^{V_C-\mathrm{Ge}V}(q_{V_C-\mathrm{Ge}V}) \tag{8}$$

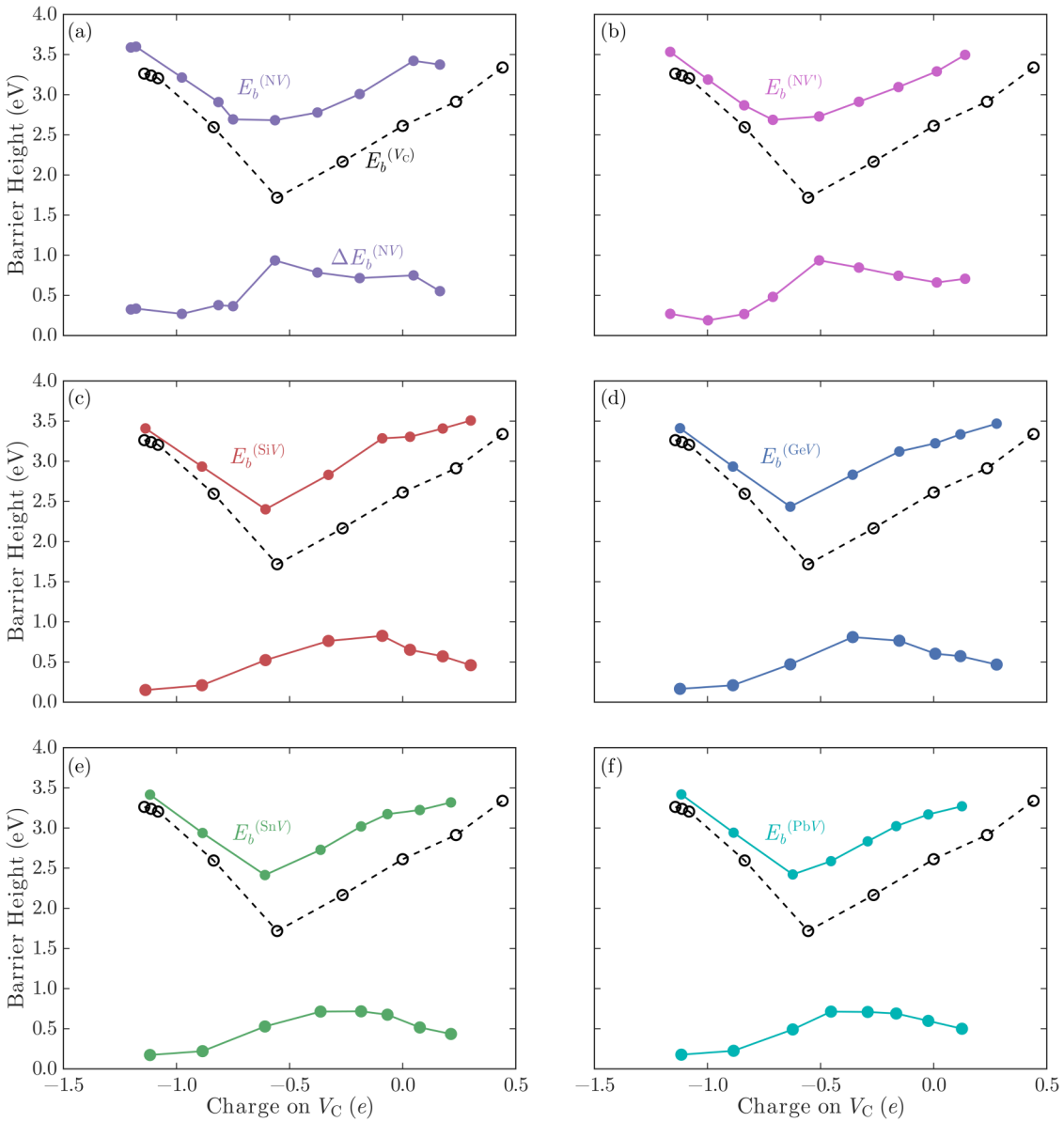

FIG. 5. Charge dependence of the barrier $E_b^{(V_C)}$ for diffusion of the isolated V_C (black open circles) and (colored dots) in the presence of (a) NV, (b) NV′, (c) SiV, (d) GeV, (e) SnV, and (f) PbV. The barrier heights for V_C near these six latter species are $E_b^{(XV)}$, where X is a particular element. The horizontal axis is the charge on the V_C. For NV′, the positions of the vacancy and the N atom have been switched to investigate the effect on the barrier of the orientation of the NV. The lines between data points are a guide to the eye. The curves at the bottom of each plot are the differences between the two barriers $\Delta E_b^{(XV)} = E_b^{(XV)} - E_b^{(V_C)}$. For the NV (NV′), the total charge values were extended down to $-8e$ and $-7e$, respectively.

so that Eq. (5) becomes

$$\Delta E_f = E_f^{V_C-GeV}(q_{V_C-GeV}) - E_f^{V_C}(q_{V_C}) - E_f^{GeV}(q_{GeV}). \quad (9)$$

Our goal is to calculate ΔE_f using Eq. (9). The term $E_f^{V_C}(q_{V_C})$ is evaluated as follows. For a fixed value of E_F, one simply calculates the formation energy for all charge states q using Eq. (1) and takes the lowest value. The same procedure is applied for GeV and V_C − GeV. Let $q^*_{V_C}$ be the charge state of V_C, q^*_{GeV} be the charge state of GeV, and $q^*_{V_C-GeV}$ be the charge state of V_C − GeV after this first step. There is no reason why this first step should lead to charge conservation in Eq. (4) as the two isolated species and the complex will necessarily form distinct bonding structures,

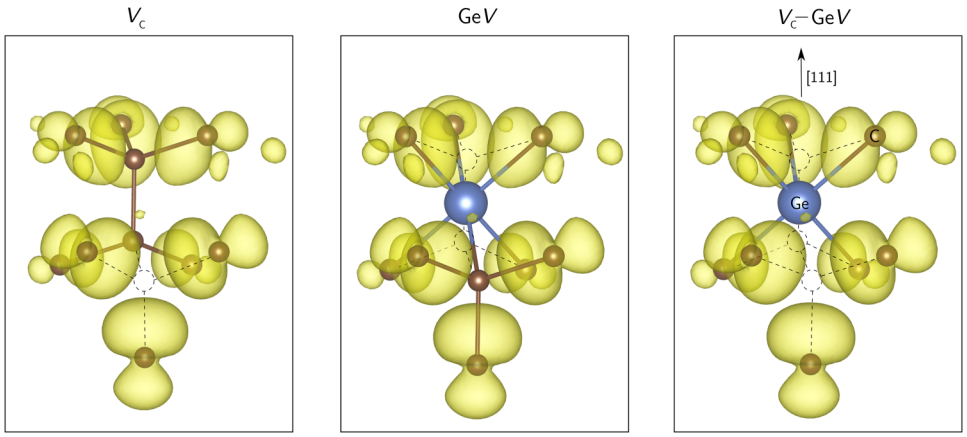

FIG. 6. Structure of the V_C defect (left), the isolated GeV center (middle), and the V_C–GeV complex (right). Carbon atoms are indicated in brown and the Ge atom in blue. The associated charge density for the V_C–GeV complex is shown to indicate where bonds are formed.

which suggests different chemical behavior. Indeed, in general, $q^*_{V_C-GeV} \neq q^*_{V_C} + q^*_{GeV}$. To rectify this imbalance, we add free electrons or holes to Eq. (4). By analogy to the case of a binary compound AB where one must consider A-rich and B-rich preparation conditions in calculating the formation energy of defects, we determine whether to add free electrons or holes to the left or the right side of Eq. (4) by considering regimes where no energy is injected into the system (energy poor) or where the supply of energy is inexhaustible (energy rich). If no energy is injected into the system, the additional electrons or holes must go to the right side of Eq. (4), while if the supply of energy is inexhaustible, the additional electrons or holes go to the left side of Eq. (4). We note that the procedure of adding free electrons or holes may reorder the formation energies, changing the charge state of the species corresponding to the minimum formation energy for the system. Thus, if we consider, for example, the regime where no energy is injected into the system, we need to consider all charge states of the $V_C - GeV$ from $q_i = q^*_{V_C-GeV}$ to $q_i = q^*_{V_C} + q^*_{GeV}$ with the appropriate addition of free electrons or holes such that charge is always conserved in the reaction. We then calculate the formation energy of the corresponding systems and take the minimum of these energies. The procedure, therefore, ensures charge conservation and that only the thermodynamically favored systems or lowest energy systems are considered.

We note that an energy poor forward reaction corresponds to the same set of formation energies as an energy rich reverse reaction and, similarly, an energy rich forward reaction is equivalent to an energy poor reverse reaction. Thus, if the system is energy poor, the forward reaction is modeled with the energy poor forward reaction and the reverse reaction is modeled with the energy rich forward reaction. We argue that no ambiguity ensues regarding the results of the reaction as follows. Given an energy poor forward reaction where the products have energy higher than the reactants, the reaction should not proceed, and there is no need to worry about whether the reverse reaction is energy rich or energy poor. If not, then the reaction will proceed. Indeed, if in the energy poor forward reaction the forward reaction product is of lower energy than the forward reaction reactants, it will necessarily be so in the energy rich forward reaction as well. Also, if the energy difference is quite great, it may even be more correct to model the reverse reaction as an energy rich reaction, so again, there is absolutely no ambiguity. We then come to the question of energy rich reactions. If the reaction is energy rich and there is a sign flip in the difference in formation energies for the reaction when considering the energy poor counterpart (which is equivalent to the energy rich reverse reaction), then we would expect both forward and reverse reactions to occur (which is indeed exactly what we should observe if the system has enough energy).

Let us generalize our discussion from the case of GeV to XV and let $q_3 = q^*_{V_C-XV}$, $q_2 = q^*_{XV}$, and $q_1 = q^*_{V_C}$. Formally, for a given value of the Fermi level in energy poor conditions, let

$$E_{f_0}^{(V_C-XV)} = \min_{q_3}\left[E_f^{(V_C-XV)}(q_3)\right] + [q_3 - (q_1 + q_2)] \cdot (E_{CBM} - E_F), \tag{10}$$

where we are minimizing over the variable q_3 in the first term (yielding the charge state labeled in the same way), the last term is included to ensure charge conservation for the case $q_3 > q_1 + q_2$ by adding the energy of $q_3 - (q_1 + q_2)$ free electrons to the right side of Eq. (9) and E_{CBM} is the absolute position of the conduction band minimum, or

$$E_{f_0}^{(V_C-XV)} = \min_{q_3}\left[E_f^{(V_C-XV)}(q_3)\right] + [(q_1 + q_2) - q_3] \cdot (E_F - E_{VBM}), \tag{11}$$

where the last term is included to ensure charge conservation for the case $q_3 < q_1 + q_2$ by adding the energy of $(q_1 + q_2) - q_3$ free holes to the right side of Eq. (9). In energy rich conditions, let

$$E_{f_0}^{(V_C+XV)} = \min_{q_1,q_2}\left[E_f^{(V_C)}(q_1) + E_f^{(XV)}(q_2)\right] + [(q_1 + q_2) - q_3] \cdot (E_{CBM} - E_F), \tag{12}$$

where we are minimizing over q_1 and q_2 in the first term (yielding similarly labeled charge states) and the last term is included to ensure charge conservation for the case $q_3 < q_1 + q_2$ by subtracting

the energy of $(q_1 + q_2) - q_3$ free electrons from the right side of Eq. (9), or

$$E_{f_0}^{(V_C+XV)} = \min_{q_1,q_2}\left[E_f^{(V_C)}(q_1) + E_f^{(XV)}(q_2)\right] + [q_3 - (q_1 + q_2)] \cdot (E_F - E_{VBM}), \quad (13)$$

where the last term is included to ensure charge conservation for the case $q_3 > q_1 + q_2$ by subtracting the energy of $q_3 - (q_1 + q_2)$ free holes from the right side of Eq. (9). Given possible reordering of the formation energies with the addition of free electrons or holes, let $i = 0, \ldots, \max[q_3 - (q_1 + q_2), 0]$ and consider

$$E_{f_i}^{(V_C-XV)} = E_f^{(V_C-XV)}(q_3 - i) + [q_3 - i - (q_1 + q_2)] \cdot (E_{CBM} - E_F) \quad (14)$$

or let $i = 0, \ldots, \max[(q_1 + q_2) - q_3, 0]$ and consider

$$E_{f_i}^{(V_C-XV)} = E_f^{(V_C-XV)}(q_3 + i) + [(q_1 + q_2) - i - q_3] \cdot (E_F - E_{VBM}) \quad (15)$$

for energy poor conditions. For energy rich conditions, let $i = 0, \ldots, \max[(q_1 + q_2) - q_3, 0]$ and consider

$$E_{f_i}^{(V_C+XV)} = \min_{q_1'+q_2'=q_1+q_2-i}\left[E_f^{(V_C)}(q_1') + E_f^{(XV)}(q_2')\right] + [(q_1 + q_2) - i - q_3] \cdot (E_{CBM} - E_F), \quad (16)$$

where we are now minimizing over the variables q_1' and q_2' in the first term or let $i = 0, \ldots, \max[q_3 - (q_1 + q_2), 0]$ and consider

$$E_{f_i}^{(V_C+XV)} = \min_{q_1'+q_2'=q_1+q_2+i}\left[E_f^{(V_C)}(q_1') + E_f^{(XV)}(q_2')\right] + [q_3 - i - (q_1 + q_2)] \cdot (E_F - E_{VBM}). \quad (17)$$

To ensure we have the lowest energy, for energy rich conditions, we take

$$\varepsilon_f^{(V_C+XV)} = \min_i\left[E_{f_i}^{(V_C+XV)}\right], \quad (18)$$

$$\varepsilon_f^{(V_C-XV)} = E_f^{(V_C-XV)}(q_3). \quad (19)$$

For energy poor conditions, we take

$$\varepsilon_f^{(V_C-XV)} = \min_i\left[E_{f_i}^{(V_C-XV)}\right], \quad (20)$$

$$\varepsilon_f^{(V_C+XV)} = E_f^{(V_C)}(q_1) + E_f^{(XV)}(q_2), \quad (21)$$

where a dependence on the Fermi level is implied. Using Eqs. (18)–(21) ensures both charge conservation and the consideration of only the thermodynamically favored products and reactants. We have analogously also calculated the quantity $\varepsilon_f^{(V_C-XV)}$ for the separation of V_C and XV by a finite distance.

In Fig. 7, we show the formation energy results for various V_C–XV complexes. These results show that the V_C easily forms complexes with the XV for most Fermi level values, ultimately depleting the yield of isolated XV color centers in diamond. We note that this spontaneity of complex formation assumes that the two species move from infinity to minimal separation without passing through any intermediate separation distances. We have only displayed results for the limiting regime where no energy is injected into the system, as that regime demonstrates the best chance of not forming complexes. The limiting regime where the supply of energy is inexhaustible has uniformly higher formation energies for the system consisting of the separated XV and V_C than for the system of the $XV - V_C$ for all species X and all values of the Fermi level. We explain the propensity to form complexes by the fact that hybridization is generally an energetically favorable process, though, for the atoms with fewer electronic orbitals such as Si and Ge, the bonding orbitals do not appear to be extended enough to support the formation of complexes once they have already been saturated with sufficient negative charge (a nonintuitive result as one might expect complexes to always form). This inability to support the formation of complexes for high Fermi level values is reflected in the fact that the solid lines jump above the dashed lines in Figs. 7(b) and 7(c). The significantly larger electronegativity of nitrogen explains its ability to continue forming complexes at high Fermi level values despite having few electronic orbitals.

Given that the two species must pass through intermediate distances in approaching one another to minimal separation from infinity, in Fig. 7, we have also explored the case of finite separation by a distance of 7.62 Å (the maximum separation between defects in a $3 \times 3 \times 3$ supercell). We emphasize that it is the difference between the lines of interest and the dashed lines in a given plot that is physically relevant to the process of the XV and V_C approaching each other to some distance given the existence of the XV and V_C species at infinity. We find a very intuitive result that may explain why we can actually experimentally observe isolated charged color centers. The result is that for Fermi level values corresponding to two similarly charged species, the energy associated with the system of the two species increases as the two species approach the finite separation from infinity. We can understand this result by recognizing the influence of repulsion of similarly charged species. Indeed, for Fermi level values where one or both of the species are neutral, the energy is no longer higher as the two species approach the finite separation from infinity. As above, we expect the energies to increase up until the minimum distance where hybridization of orbitals is no longer experienced and then decrease thereafter, other than when one or more of the species is neutral in which case polarization effects must be taken into account. Based on Fig. 5, the fact that the V_C are more likely to get stuck as they approach the color center for low Fermi level values and thus be impeded in further motion may explain the ability to form neutral color centers despite thermodynamic results suggesting the contrary.

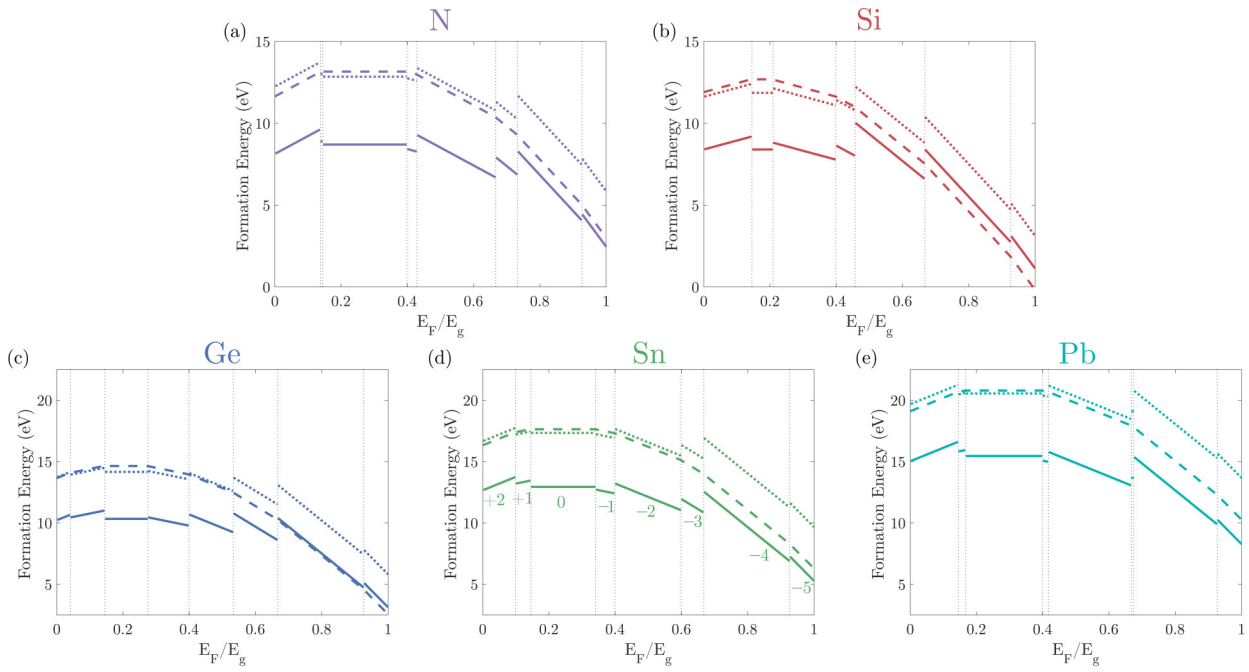

FIG. 7. Formation energy $\varepsilon_f^{(V_C-XV)}$ for the V_C-XV complex (solid lines), $\varepsilon_f^{(V_C+XV)}$ for V_C and XV separated by an infinite distance (dashed lines), and $\varepsilon_f^{(V_C-XV)}$ for V_C and XV separated by a finite distance (dotted lines), for (a) X = N, (b) X = Si, (c) X = Ge, (d) X = Sn, and (e) X = Pb. Vertical dotted lines indicate transitions between charge states. Formation energies are shown for the regime where no energy is injected into the system. The inexhaustible supply of energy regime is not displayed.

F. The effect of V_C on acoustic phonons

We finally turn to the question of how best to deal with a mechanism that can be detrimental to the performance of XV^- color centers in diamond, namely, the effect of acoustic phonons. As the mass of the X element in a XV^- color center is increased in going from Si to Ge to Sn, and finally to Pb, the enhanced spin–orbit coupling of the heavier elements causes a larger energy level splitting in the ground state.[34] This observation is relevant as it is well known that acoustic phonons can interact with the lighter XV^- color centers on the energy scale of the ground state or orbital splitting frequency, thus disrupting the coherence times of the spin states of these XV^- color centers at higher temperatures.[19,23] Any proposal to increase the spin coherence time of color centers must clearly address the matter of the prevalence of acoustic phonons in the host material. It has been suggested that by decreasing the phonon density of states (PDOS) $g(\omega)$ about the orbital splitting frequency of XV^- color centers, one can enhance their spin coherence times.[19] For the XV^- color centers under investigation, these frequencies lie below 2.5 THz.[19,34,49,87,88]

Let us consider a simple model in which we propose a way to decrease the number of acoustic phonons in the bulk material by modulating the V_C density in the host material. We will first show that for a simple cubic lattice, the PDOS is proportional to the inverse of the primitive unit cell volume V_{pc} as the frequency goes to zero. Explicitly, using the Debye model for a 3D crystal, the PDOS per unit volume $\tilde{g}(\omega)$ is[89,90]

$$\tilde{g}(\omega) = \frac{3}{2\pi^2}\frac{\omega^2}{v^3}, \tag{22}$$

where $v = \omega_D\left(\frac{\Omega}{2\pi^2 N_{ph}}\right)^{(1/3)}$ is the speed of sound, ω_D is the Debye frequency, N_{ph} is the number of available acoustic phonon modes ($N_{ph} = 3N$, where N is the number of primitive unit cells in the crystal), and Ω is the volume of the crystal. Upon multiplying Eq. (22) by the volume of the crystal Ω, we obtain an expression for the PDOS,

$$g(\omega) = 9N\frac{\omega^2}{\omega_D^3}. \tag{23}$$

Since the number of primitive unit cells, N, is inversely proportional to V_{pc} for a fixed crystal size, we have proved our desired result. We note here that such an approximation is valid for small frequencies, where the phonon dispersion relation can be approximated as linear.

Then, if the size of the primitive unit cell can be increased relative to the size of the crystal, the density of phonons for low frequencies would decrease. A simple way to increase V_{pc} would be

to have a diamond lattice with a very small but nonzero number of defects. As the color center already constitutes one defect, the ideal scenario would be to have no V_C. Essentially, if the number of defects were zero, the unit cell would reduce to the proper unit cell of diamond, but if there is a single defect in the crystal, the unit cell should then increase to the size of the crystal. Roughly speaking, for uniformly distributed defects in the crystal, the size of the unit cell should be about the size of the crystal divided by the number of defects, and the phonon density of states near zero frequency should then increase or decrease correspondingly. In a different problem entirely equivalent to the one discussed here, it has been shown that the waves scattered off a system with subwavelength patterning can be solved with good accuracy by modeling each region of the system as one being reproduced periodically throughout the system, solving for the waves from that region, and then stitching the solutions together.[91] We therefore argue that the phonon behavior should be determined to acceptable accuracy based on local densities of defects in the physically realized systems.

In Fig. 8, using the Phonopy code,[77] we investigate the effect of changing the density of the V_C in the diamond lattice on the PDOS by considering five different 64-atom supercells of varying defect densities: a supercell with no vacancies, two distinct supercells each containing 16 vacancies located in two different configurations, a supercell with 8 vacancies, and a supercell with 1 vacancy. For the supercell with 1 vacancy (green), the vacancy was placed at the carbon site located at (0, 0, 0) in the supercell. For the supercell with 8 vacancies (red), the vacancies were generated by placing a vacancy at the carbon site located at the (0, 0, 0) position of the conventional unit cell of diamond, which was then periodically repeated throughout the supercell to generate all eight vacancies. As a representative test of the idea that it is indeed the size of the smallest effectively periodic unit that affects the PDOS, we also created two supercells with 16 vacancies. In one, the vacancies were placed at the carbon sites located at (0, 0, 0) and (0.25, 0.25, 0.25) (purple) positions of the conventional unit cell of diamond, and in the other, the vacancies were placed at the carbon sites located at (0, 0, 0) and (0.5, 0.5, 0) (gold) positions of the conventional unit cell of diamond, both in units of the lattice constant of the conventional unit cell. These two conventional unit cells were then periodically repeated throughout the supercell to generate two distinct configurations of 16 vacancies. We see that the phonon density of states is effectively zero at low frequencies for the smallest nonzero defect density $\frac{1\,V_C}{\text{supercell}}$ and increases as the density of defects is increased. The pronounced increase for a curve corresponding to $\frac{16\,V_C}{\text{supercell}}$ (in gold) over the other curve corresponding to $\frac{16\,V_C}{\text{supercell}}$ (in purple) is due to the following effect: For the latter structure, the second vacancy in a conventional unit cell was placed as close as possible to the first vacancy resulting in very little change in the effective periodicity of the cell, while for the former structure, it was placed as far as possible from the first vacancy, thus roughly halving the conventional unit cell along certain directions with a corresponding increase in the phonon density of states at low frequencies.

In Fig. 9, again using the Phonopy code,[77] we have examined the phonon density of states using a supercell consisting of either a single SiV^- or a single GeV^-. We propose to use the results of Fig. 9 to explain the fact that the GeV^- has a spin coherence time equal to or less than that of the SiV^- despite having a larger ground state splitting.[92] Given that the systems we are dealing with consist of electronic spins, for a total spin S, the corresponding system will involve a number of entangled electrons n_e at least equal to $2S$. Thus, since the Larmor frequency is inversely proportional to the mass of the system, under an external field, the spin of

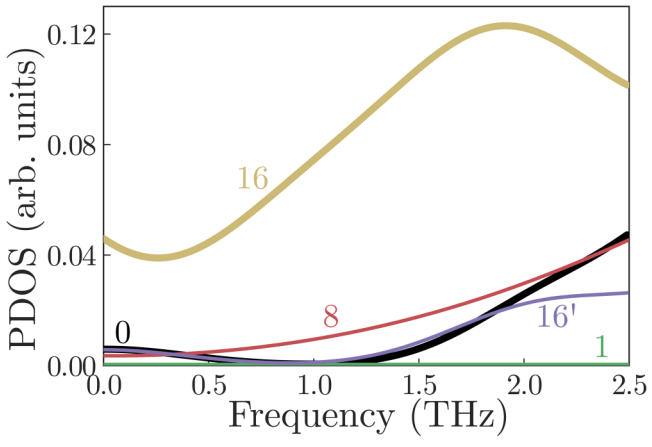

FIG. 8. Phonon density of states for various V_C concentrations and positions in the diamond lattice, as described in the text. The labels of the various curves correspond to the number of V_C defects in a 64-atom supercell. For supercell configurations that have a nonzero density of V_C and that have the V_C roughly uniformly distributed in the supercell, we observe an increase in the PDOS at low frequency as the density is increased. The primed number indicates a configuration where the distribution of V_C deviated significantly from uniform.

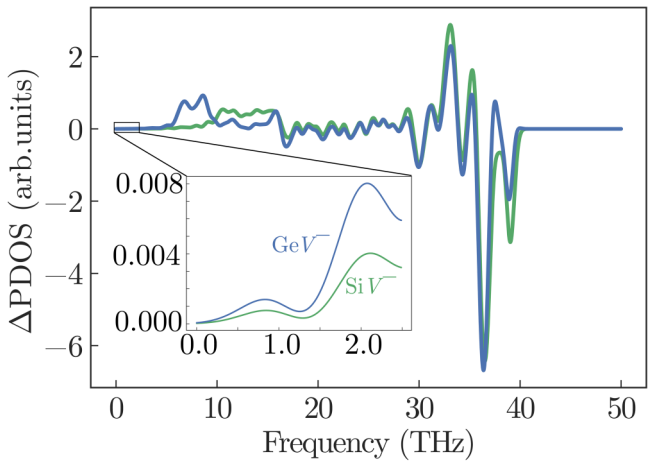

FIG. 9. Difference between the phonon density of states for a $3 \times 3 \times 3$ supercell system containing a single SiV^- and for stoichiometric diamond (green) and for a $3 \times 3 \times 3$ supercell system containing a single GeV^- and for stoichiometric diamond (blue). One notes that for the low frequencies (until roughly 10 THz), the GeV^- curve is consistently higher than the SiV^- curve.

the system will precess with a Larmor frequency suppressed by a factor of $n_e m_e$, where m_e is the mass of the electron. As the total spin increases, n_e increases, implying that the spin will rotate out of phase more slowly. Indeed, Childress *et al.*[93] found suppressed decoherence when NV^- spins were entangled with the much more massive ^{13}C nuclear spins. One might then imagine that for systems with the same total spin and the same environment, the bulk of the difference in the spin coherence time might be explained by deferring to ground state splitting. However, as alluded to above, this explanation does not work for the SiV^- and GeV^-. We make a further simple observation that for a field that is periodically varying with frequency ω_B, the change in the angle of the spin with time will be suppressed by a factor of ω_B, obtained by integrating the expression for the Larmor frequency. Thus, the fluctuating fields associated with phonons with high enough frequencies will be unable to rotate the color center spin completely out of phase, suggesting that we should predominantly consider the low frequency regime in comparing the GeV^- and SiV^- phonon densities. Indeed, in that regime, GeV^- has a higher phonon density than SiV^-, which we propose would explain its equal or shorter spin coherence time despite the larger ground state splitting.

IV. CONCLUSIONS

Single carbon vacancies can have a deleterious effect on the spin and optical properties of isolated Group IV color centers (XV) in diamond, where X = Si, Ge, Sn, and Pb and V is a carbon vacancy. In an effort to understand the thermodynamics and kinetics of how a single carbon vacancy-XV complex (V_C−XV) is created, we used DFT to compute the formation energies and charge transition levels for both V_C and each of the four individual Group IV color centers, the diffusion barrier height $E_b^{(V_C)}$ for isolated V_C, and the diffusion barrier $E_b^{(XV)}$ for V_C in the proximity in each of these four XV color centers. We have also demonstrated the dependence of both $E_b^{(V_C)}$ and $E_b^{(XV)}$ on the Fermi level of the host diamond material and have computed the formation energy for a V_C−XV complex while conserving charge. All of this information can be used as an experimental guide on how to dope or apply an electric bias to samples in order to reversibly tune the Fermi level to the appropriate regime where diffusion of V_C toward a given color center would be impeded or rendered energetically unfavorable for the formation of a V_C−XV complex. By better isolating color centers from the V_C defects and thus reducing the prevalence of acoustic phonons, we expect that the spin coherence times for XV color centers would be enhanced. Finally, we note that all of these results involving XV color centers are applicable to NV centers in diamond.

ACKNOWLEDGMENTS

R.K.D. gratefully acknowledges financial support from the IACS Student Scholarship. We also acknowledge support by the STC Center for Integrated Quantum Materials, National Science Foundation (NSF) (Grant No. DMR-1231319) and the NSF-ECCS-1748106 EAGER grant. This work used computational resources of the Extreme Science and Engineering Discovery Environment (XSEDE), which is supported by the National Science Foundation (Grant No. ACI-1548562[94]), on Stampede2 at TACC through Allocation No. TG-DMR120073, and of the National Energy Research Scientific Computing Center (NERSC), a U.S. Department of Energy Office of Science User Facility operated under Contract No. DE-AC02-05CH11231. We would like to thank Marko Lončar for bringing our attention to Ref. 49 when it was in the form of a preprint. We also thank Diana Prado Lopes Aude Craik, Smarak Maity, Linbo Shao, and Michael Walsh for very useful experimental discussions on the creation of V_C in diamond by ion implantation and on the properties of NV and Group IV color centers as well. Finally, we thank Pratibha Dev for useful theoretical discussions regarding the convergence of the results.

REFERENCES

[1]M. W. Doherty, N. B. Manson, P. Delaney, F. Jelezko, J. Wrachtrup, and L. C. Hollenberg, "The nitrogen-vacancy colour centre in diamond," Phys. Rep. **528**, 1 (2013).
[2]P. Deák, B. Aradi, M. Kaviani, T. Frauenheim, and A. Gali, "Formation of NV centers in diamond: A theoretical study based on calculated transitions and migration of nitrogen and vacancy related defects," Phys. Rev. B **89**, 075203 (2014).
[3]A. Gali, E. Janzén, P. Deák, G. Kresse, and E. Kaxiras, "Theory of spin-conserving excitation of the $N-V^-$ center in diamond," Phys. Rev. Lett. **103**, 186404 (2009).
[4]D. D. Awschalom, R. Hanson, J. Wrachtrup, and B. B. Zhou, "Quantum technologies with optically interfaced solid-state spins," Nat. Photon. **12**, 516 (2018).
[5]R. Kuate Defo, R. Wang, and M. Manjunathaiah, "Parallel BFS implementing optimized decomposition of space and kMC simulations for diffusion of vacancies for quantum storage," J. Comput. Sci. **36**, 101018 (2019).
[6]R. Kuate Defo, X. Zhang, D. Bracher, G. Kim, E. Hu, and E. Kaxiras, "Energetics and kinetics of vacancy defects in 4*H*-SiC," Phys. Rev. B **98**, 104103 (2018).
[7]N. Bar-Gill, L. M. Pham, A. Jarmola, D. Budker, and R. L. Walsworth, "Solid-state electronic spin coherence time approaching one second," Nat. Commun. **4**, 1743 (2013).
[8]G. Balasubramanian, P. Neumann, D. Twitchen, M. Markham, R. Kolesov, N. Mizuochi, J. Isoya, J. Achard, J. Beck, J. Tissler, V. Jacques, P. R. Hemmer, F. Jelezko, and J. Wrachtrup, "Ultralong spin coherence time in isotopically engineered diamond," Nat. Mater. **8**, 383 (2009).
[9]M. H. Abobeih, J. Cramer, M. A. Bakker, N. Kalb, M. Markham, D. J. Twitchen, and T. H. Taminiau, "One-second coherence for a single electron spin coupled to a multi-qubit nuclear-spin environment," Nat. Commun. **9**, 2552 (2018).
[10]F. Jelezko, C. Tietz, A. Gruber, I. Popa, A. Nizovtsev, S. Kilin, and J. Wrachtrup, "Spectroscopy of single N-V centers in diamond," Single Mol. **2**, 255 (2001).
[11]A. Zaitsev, V. Vavilov, and A. Gippius, "Cathodoluminescence of diamond associated with silicon impurity," Sov. Phys. Lebedev Inst. Rep. **10**, 15 (1981).
[12]J. P. Goss, R. Jones, S. J. Breuer, P. R. Briddon, and S. Öberg, "The twelve-line 1.682 eV luminescence center in diamond and the vacancy-silicon complex," Phys. Rev. Lett. **77**, 3041 (1996).
[13]C. D. Clark, H. Kanda, I. Kiflawi, and G. Sittas, "Silicon defects in diamond," Phys. Rev. B **51**, 16681 (1995).
[14]A. Gali and J. R. Maze, "Ab initio study of the split silicon-vacancy defect in diamond: Electronic structure and related properties," Phys. Rev. B **88**, 235205 (2013).
[15]E. Neu, D. Steinmetz, J. Riedrich-Möller, S. Gsell, M. Fischer, M. Schreck, and C. Becher, "Single photon emission from silicon-vacancy colour centres in chemical vapour deposition nano-diamonds on iridium," New J. Phys. **13**, 025012 (2011).
[16]C. Hepp, T. Müller, V. Waselowski, J. N. Becker, B. Pingault, H. Sternschulte, D. Steinmüller-Nethl, A. Gali, J. R. Maze, M. Atatüre, and C. Becher, "Electronic

structure of the silicon vacancy color center in diamond," Phys. Rev. Lett. **112**, 036405 (2014).
[17]L. J. Rogers, K. D. Jahnke, M. H. Metsch, A. Sipahigil, J. M. Binder, T. Teraji, H. Sumiya, J. Isoya, M. D. Lukin, P. Hemmer, and F. Jelezko, "All-optical initialization, readout, and coherent preparation of single silicon-vacancy spins in diamond," Phys. Rev. Lett. **113**, 263602 (2014).
[18]A. Sipahigil, K. D. Jahnke, L. J. Rogers, T. Teraji, J. Isoya, A. S. Zibrov, F. Jelezko, and M. D. Lukin, "Indistinguishable photons from separated silicon-vacancy centers in diamond," Phys. Rev. Lett. **113**, 113602 (2014).
[19]B. Pingault, D.-D. Jarausch, C. Hepp, L. Klintberg, J. N. Becker, M. Markham, C. Becher, and M. Atatüre, "Coherent control of the silicon-vacancy spin in diamond," Nat. Commun. **8**, 15579 (2017).
[20]B. Pingault, J. N. Becker, C. H. H. Schulte, C. Arend, C. Hepp, T. Godde, A. I. Tartakovskii, M. Markham, C. Becher, and M. Atatüre, "All-optical formation of coherent dark states of silicon-vacancy spins in diamond," Phys. Rev. Lett. **113**, 263601 (2014).
[21]A. Dietrich, K. D. Jahnke, J. M. Binder, T. Teraji, J. Isoya, L. J. Rogers, and F. Jelezko, "Isotopically varying spectral features of silicon-vacancy in diamond," New J. Phys. **16**, 113019 (2014).
[22]J. N. Becker, J. Görlitz, C. Arend, M. Markham, and C. Becher, "Ultrafast all-optical coherent control of single silicon vacancy colour centres in diamond," Nat. Commun. **7**, 13512 (2016).
[23]K. D. Jahnke, A. Sipahigil, J. M. Binder, M. W. Doherty, M. Metsch, L. J. Rogers, N. B. Manson, M. D. Lukin, and F. Jelezko, "Electron–phonon processes of the silicon-vacancy centre in diamond," New J. Phys. **17**, 043011 (2015).
[24]D. D. Sukachev, A. Sipahigil, C. T. Nguyen, M. K. Bhaskar, R. E. Evans, F. Jelezko, and M. D. Lukin, "Silicon-vacancy spin qubit in diamond: A quantum memory exceeding 10 ms with single-shot state readout," Phys. Rev. Lett. **119**, 223602 (2017).
[25]J. N. Becker, B. Pingault, D. Groß, M. Gündoğan, N. Kukharchyk, M. Markham, A. Edmonds, M. Atatüre, P. Bushev, and C. Becher, "All-optical control of the silicon-vacancy spin in diamond at millikelvin temperatures," Phys. Rev. Lett. **120**, 053603 (2018).
[26]C. T. Nguyen, R. E. Evans, A. Sipahigil, M. K. Bhaskar, D. D. Sukachev, V. N. Agafonov, V. A. Davydov, L. F. Kulikova, F. Jelezko, and M. D. Lukin, "All-optical nanoscale thermometry with silicon-vacancy centers in diamond," Appl. Phys. Lett. **112**, 203102 (2018).
[27]U. F. S. D'Haenens-Johansson, A. M. Edmonds, B. L. Green, M. E. Newton, G. Davies, P. M. Martineau, R. U. A. Khan, and D. J. Twitchen, "Optical properties of the neutral silicon split-vacancy center in diamond," Phys. Rev. B **84**, 245208 (2011).
[28]B. C. Rose, D. Huang, Z.-H. Zhang, P. Stevenson, A. M. Tyryshkin, S. Sangtawesin, S. Srinivasan, L. Loudin, M. L. Markham, A. M. Edmonds, D. J. Twitchen, S. A. Lyon, and N. P. de Leon, "Observation of an environmentally insensitive solid-state spin defect in diamond," Science **361**, 60 (2018).
[29]K. Iakoubovskii and A. Stesmans, "Characterization of hydrogen and silicon-related defects in CVD diamond by electron spin resonance," Phys. Rev. B **66**, 195207 (2002).
[30]A. M. Edmonds, M. E. Newton, P. M. Martineau, D. J. Twitchen, and S. D. Williams, "Electron paramagnetic resonance studies of silicon-related defects in diamond," Phys. Rev. B **77**, 245205 (2008).
[31]G. Thiering and A. Gali, "The $(e_g \otimes e_u) \otimes E_g$ product Jahn–Teller effect in the neutral group-IV vacancy quantum bits in diamond," npj Comput. Mater. **5**, 18 (2019).
[32]M. H. Metsch, K. Senkalla, B. Tratzmiller, J. Scheuer, M. Kern, J. Achard, A. Tallaire, M. B. Plenio, P. Siyushev, and F. Jelezko, "Initialization and readout of nuclear spins via a negatively charged silicon-vacancy center in diamond," Phys. Rev. Lett. **122**, 190503 (2019).
[33]Y.-I. Sohn, S. Meesala, B. Pingault, H. A. Atikian, J. Holzgrafe, M. Gündoğan, C. Stavrakas, M. J. Stanley, A. Sipahigil, J. Choi, M. Zhang, J. L. Pacheco, J. Abraham, E. Bielejec, M. D. Lukin, M. Atatüre, and M. Lončar, "Controlling the coherence of a diamond spin qubit through its strain environment," Nat. Commun. **9**, 2012 (2018).
[34]T. Iwasaki, Y. Miyamoto, T. Taniguchi, P. Siyushev, M. H. Metsch, F. Jelezko, and M. Hatano, "Tin-vacancy quantum emitters in diamond," Phys. Rev. Lett. **119**, 253601 (2017).
[35]T. Iwasaki, F. Ishibashi, Y. Miyamoto, Y. Doi, S. Kobayashi, T. Miyazaki, K. Tahara, K. D. Jahnke, L. J. Rogers, B. Naydenov, F. Jelezko, S. Yamasaki, S. Nagamachi, T. Inubushi, N. Mizuochi, and M. Hatano, "Germanium-vacancy single color centers in diamond," Sci. Rep. **5**, 12882 (2015).
[36]V. G. Ralchenko, V. S. Sedov, A. A. Khomich, V. S. Krivobok, S. N. Nikolaev, S. Savin, I. I. Vlasov, and V. I. Konov, "Observation of the Ge-vacancy color center in microcrystalline diamond films," Bull. Lebedev Phys. Inst. **42**, 165 (2015).
[37]E. A. Ekimov, S. G. Lyapin, K. N. Boldyrev, M. V. Kondrin, R. Khmelnitskiy, V. A. Gavva, T. V. Kotereva, and M. N. Popova, "Germanium–vacancy color center in isotopically enriched diamonds synthesized at high pressures," JETP Lett. **102**, 701 (2015).
[38]Y. N. Palyanov, I. N. Kupriyanov, Y. M. Borzdov, and N. V. Surovtsev, "Germanium: A new catalyst for diamond synthesis and a new optically active impurity in diamond," Sci. Rep. **5**, 14789 (2015).
[39]Y. N. Palyanov, I. N. Kupriyanov, Y. M. Borzdov, A. F. Khokhryakov, and N. V. Surovtsev, "High-pressure synthesis and characterization of Ge-doped single crystal diamond," Cryst. Growth Des. **16**, 3510 (2016).
[40]E. A. Ekimov, V. S. Krivobok, S. G. Lyapin, P. S. Sherin, V. A. Gavva, and M. V. Kondrin, "Anharmonicity effects in impurity-vacancy centers in diamond revealed by isotopic shifts and optical measurements," Phys. Rev. B **95**, 094113 (2017).
[41]M. K. Bhaskar, D. D. Sukachev, A. Sipahigil, R. E. Evans, M. J. Burek, C. T. Nguyen, L. J. Rogers, P. Siyushev, M. H. Metsch, H. Park, F. Jelezko, M. Lončar, and M. D. Lukin, "Quantum nonlinear optics with a germanium-vacancy color center in a nanoscale diamond waveguide," Phys. Rev. Lett. **118**, 223603 (2017).
[42]K. Bray, B. Regan, A. Trycz, R. Previdi, G. Seniutinas, K. Ganesan, M. Kianinia, S. Kim, and I. Aharonovich, "Single crystal diamond membranes and photonic resonators containing germanium vacancy color centers," ACS Photonics **5**, 4817 (2018).
[43]E. Ekimov, M. Kondrin, V. Krivobok, A. Khomich, I. Vlasov, R. Khmelnitskiy, T. Iwasaki, and M. Hatano, "Effect of Si, Ge and Sn dopant elements on structure and photoluminescence of nano- and microdiamonds synthesized from organic compounds," Diam. Relat. Mater. **93**, 75 (2019).
[44]S. Ditalia Tchernij, T. Herzig, J. Forneris, J. Küpper, S. Pezzagna, P. Traina, E. Moreva, I. P. Degiovanni, G. Brida, N. Skukan, M. Genovese, M. Jakšić, J. Meijer, and P. Olivero, "Single-photon-emitting optical centers in diamond fabricated upon Sn implantation," ACS Photonics **4**, 2580 (2017).
[45]E. Ekimov, S. Lyapin, and M. Kondrin, "Tin-vacancy color centers in micro- and polycrystalline diamonds synthesized at high pressures," Diam. Relat. Mater. **87**, 223 (2018).
[46]Y. N. Palyanov, I. N. Kupriyanov, and Y. M. Borzdov, "High-pressure synthesis and characterization of Sn-doped single crystal diamond," Carbon **143**, 769 (2019).
[47]M. Alkahtani, I. Cojocaru, X. Liu, T. Herzig, J. Meijer, J. Küpper, T. Lühmann, A. V. Akimov, and P. R. Hemmer, "Tin-vacancy in diamonds for luminescent thermometry," Appl. Phys. Lett. **112**, 241902 (2018).
[48]A. E. Rugar, C. Dory, S. Sun, and J. Vučković, "Characterization of optical and spin properties of single tin-vacancy centers in diamond nanopillars," Phys. Rev. B **99**, 205417 (2019).
[49]M. E. Trusheim, N. H. Wan, K. C. Chen, C. J. Ciccarino, J. Flick, R. Sundararaman, G. Malladi, E. Bersin, M. Walsh, B. Lienhard, H. Bakhru, P. Narang, and D. Englund, "Lead-related quantum emitters in diamond," Phys. Rev. B **99**, 075430 (2019).
[50]S. Ditalia Tchernij, T. Lühmann, T. Herzig, J. Küpper, A. Damin, S. Santonocito, M. Signorile, P. Traina, E. Moreva, F. Celegato, S. Pezzagna, I. P. Degiovanni, P. Olivero, M. Jakšić, J. Meijer, P. M. Genovese, and J. Forneris, "Single-photon emitters in lead-implanted single-crystal diamond," ACS Photonics **5**, 4864 (2018).
[51]G. Thiering and A. Gali, "*Ab initio* magneto-optical spectrum of Group-IV vacancy color centers in diamond," Phys. Rev. X **8**, 021063 (2018).

[52]J. Meijer, B. Burchard, M. Domhan, C. Wittmann, T. Gaebel, I. Popa, F. Jelezko, and J. Wrachtrup, "Generation of single color centers by focused nitrogen implantation," Appl. Phys. Lett. **87**, 261909 (2005).
[53]S. Pezzagna, B. Naydenov, F. Jelezko, J. Wrachtrup, and J. Meijer, "Creation efficiency of nitrogen-vacancy centres in diamond," New J. Phys. **12**, 065017 (2010).
[54]J. Rabeau, P. Reichart, G. Tamanyan, D. Jamieson, S. Prawer, F. Jelezko, T. Gaebel, I. Popa, M. Domhan, and J. Wrachtrup, "Implantation of labelled single nitrogen vacancy centers in diamond using ^{15}N," Appl. Phys. Lett. **88**, 023113 (2006).
[55]C. D. Weis, A. Schuh, A. Batra, A. Persaud, I. W. Rangelow, J. Bokor, C. C. Lo, S. Cabrini, E. Sideras-Haddad, G. Fuchs *et al.*, "Single atom doping for quantum device development in diamond and silicon," J. Vac. Sci. Technol. B **26**, 2596 (2008).
[56]T. Lühmann, N. Raatz, R. John, M. Lesik, J. Rödiger, M. Portail, D. Wildanger, F. Kleißler, K. Nordlund, A. Zaitsev, J.-F. Roch, A. Tallaire, J. Meijer, and S. Pezzagna, "Screening and engineering of colour centres in diamond," J. Phys. D: Appl. Phys. **51**, 483002 (2018).
[57]J. Schwartz, P. Michaelides, C. Weis, and T. Schenkel, "*In situ* optimization of co-implantation and substrate temperature conditions for nitrogen-vacancy center formation in single-crystal diamonds," New J. Phys. **13**, 035022 (2011).
[58]B. Naydenov, V. Richter, J. Beck, M. Steiner, P. Neumann, G. Balasubramanian, J. Achard, F. Jelezko, J. Wrachtrup, and R. Kalish, "Enhanced generation of single optically active spins in diamond by ion implantation," Appl. Phys. Lett. **96**, 163108 (2010).
[59]T. Yamamoto, T. Umeda, K. Watanabe, S. Onoda, M. L. Markham, D. J. Twitchen, B. Naydenov, L. P. McGuinness, T. Teraji, S. Koizumi, F. Dolde, H. Fedder, J. Honert, J. Wrachtrup, T. Ohshima, F. Jelezko, and J. Isoya, "Extending spin coherence times of diamond qubits by high-temperature annealing," Phys. Rev. B **88**, 075206 (2013).
[60]L. Hounsome, R. Jones, P. Martineau, M. Shaw, P. Briddon, S. Öberg, A. Blumenau, and N. Fujita, "Optical properties of vacancy related defects in diamond," Phys. Status Solidi A **202**, 2182–2187 (2005).
[61]K. Iakoubovskii and A. Stesmans, "Vacancy clusters in diamond studied by electron spin resonance," Phys. Status Solidi A **201**, 2509–2515 (2004).
[62]F. Fávaro de Oliveira, D. Antonov, Y. Wang, P. Neumann, S. A. Momenzadeh, T. Häußermann, A. Pasquarelli, A. Denisenko, and J. Wrachtrup, "Tailoring spin defects in diamond by lattice charging," Nat. Commun. **8**, 15409 (2017).
[63]G. Kresse and J. Hafner, "*Ab initio* molecular dynamics for liquid metals," Phys. Rev. B **47**, 558 (1993).
[64]G. Kresse and J. Furthmüller, "Efficient iterative schemes for *ab initio* total-energy calculations using a plane-wave basis set," Phys. Rev. B **54**, 11169 (1996).
[65]G. Kresse and D. Joubert, "From ultrasoft pseudopotentials to the projector augmented-wave method," Phys. Rev. B **59**, 1758 (1999).
[66]J. P. Perdew, K. Burke, and M. Ernzerhof, "Generalized gradient approximation made simple," Phys. Rev. Lett. **77**, 3865 (1996).
[67]S. B. Zhang and J. E. Northrup, "Chemical potential dependence of defect formation energies in GaAs: Application to Ga self-diffusion," Phys. Rev. Lett. **67**, 2339 (1991).
[68]C. Freysoldt, B. Grabowski, T. Hickel, J. Neugebauer, G. Kresse, A. Janotti, and C. G. Van de Walle, "First-principles calculations for point defects in solids," Rev. Mod. Phys. **86**, 253 (2014).
[69]D. Vinichenko, M. G. Sensoy, C. M. Friend, and E. Kaxiras, "Accurate formation energies of charged defects in solids: A systematic approach," Phys. Rev. B **95**, 235310 (2017).
[70]G. Henkelman, B. P. Uberuaga, and H. Jãnsson, "A climbing image nudged elastic band method for finding saddle points and minimum energy paths," J. Chem. Phys. **113**, 9901 (2000).
[71]H. Jãnsson, G. Mills, and K. W. Jacobsen, "Nudged elastic band method for finding minimum energy paths of transitions," in *Classical and Quantum Dynamics in Condensed Phase Simulations* (World Scientific, Singapore, 1998), pp. 385–404.
[72]A. F. Voter, "Introduction to the kinetic Monte Carlo method," in *Radiation Effects in Solids*, edited by K. E. Sickafus, E. A. Kotomin, and B. P. Uberuaga (Springer Netherlands, Dordrecht, 2007), pp. 1–23.
[73]T. A. Manz and N. G. Limas, "Introducing DDEC6 atomic population analysis: Part 1. Charge partitioning theory and methodology," RSC Adv. **6**, 47771 (2016).
[74]T. A. Manz and D. S. Sholl, "Chemically meaningful atomic charges that reproduce the electrostatic potential in periodic and nonperiodic materials," J. Chem. Theory Comput. **6**, 2455 (2010).
[75]W. Cao, C. Gatti, P. MacDougall, and R. Bader, "On the presence of non-nuclear attractors in the charge distributions of Li and Na clusters," Chem. Phys. Lett. **141**, 380 (1987).
[76]A. E. Reed, R. B. Weinstock, and F. Weinhold, "Natural population analysis," J. Chem. Phys. **83**, 735 (1985).
[77]A. Togo and I. Tanaka, "First principles phonon calculations in materials science," Scr. Mater. **108**, 1 (2015).
[78]M. E. Levinshtein, S. L. Rumyantsev, and M. S. Shur, *Properties of Advanced Semiconductor Materials: GaN, AlN, InN, BN, SiC, SiGe* (John Wiley & Sons, Inc., New York, 2001).
[79]J. Isberg, J. Hammersberg, E. Johansson, T. Wikström, D. J. Twitchen, A. J. Whitehead, S. E. Coe, and G. A. Scarsbrook, "High carrier mobility in single-crystal plasma-deposited diamond," Science **297**, 1670 (2002).
[80]S. Salustro, A. M. Ferrari, R. Orlando, and R. Dovesi, "Comparison between cluster and supercell approaches: The case of defects in diamond," Theor. Chem. Acc. **136**, 42 (2017).
[81]A. Zelferino, S. Salustro, J. Baima, V. Lacivita, R. Orlando, and R. Dovesi, "The electronic states of the neutral vacancy in diamond: A quantum mechanical approach," Theor. Chem. Acc. **135**, 74 (2016).
[82]T. Miyazaki, "Theoretical studies of sulfur and sulfur-hydrogen complexes in diamond," Phys. Status Solidi A **193**, 395 (2002).
[83]A. T. Collins, "The Fermi level in diamond," J. Phys.: Condens. Matter **14**, 3743 (2002).
[84]S. Lany and A. Zunger, "Assessment of correction methods for the band-gap problem and for finite-size effects in supercell defect calculations: Case studies for ZnO and GaAs," Phys. Rev. B **78**, 235104 (2008).
[85]K. Jacobs and F. A. Kröger, "The chemistry of imperfect crystals. 2nd revised edition, volume 1: Preparation, purification, crystal growth and phase theory. North-Holland Publishing Company—Amsterdam/London 1973 American Elsevier Publishing Company, Inc.—New York 313 Seiten, zahlreiche Abbildungen und Tabellen, Kunstleder Preis Dfl. 70.00," Krist. Tech. **9**, K67 (1974).
[86]T. Stix, *Waves in Plasmas* (American Institute of Physics, 1992).
[87]A. Gali, M. Fyta, and E. Kaxiras, "*Ab initio* supercell calculations on nitrogen-vacancy center in diamond: Electronic structure and hyperfine tensors," Phys. Rev. B **77**, 155206 (2008).
[88]P. Siyushev, M. H. Metsch, A. Ijaz, J. M. Binder, M. K. Bhaskar, D. D. Sukachev, A. Sipahigil, R. E. Evans, C. T. Nguyen, M. D. Lukin, P. R. Hemmer, Y. N. Palyanov, I. N. Kupriyanov, Y. M. Borzdov, L. J. Rogers, and F. Jelezko, "Optical and microwave control of germanium-vacancy center spins in diamond," Phys. Rev. B **96**, 081201 (2017).
[89]E. Kaxiras, *Atomic and Electronic Structure of Solids* (Cambridge University Press, 2003).
[90]N. Ashcroft and N. Mermin, *Solid State Physics* (Holt, Rinehart and Winston, 1976), HRW international editions.
[91]R. Pestourie, C. Pérez-Arancibia, Z. Lin, W. Shin, F. Capasso, and S. G. Johnson, "Inverse design of large-area metasurfaces," Opt. Express **26**, 33732 (2018).
[92]Y. Zhou, Z. Mu, G. Adamo, S. Bauerdick, A. Rudzinski, I. Aharonovich, and W. Gao, "Direct writing of single germanium vacancy center arrays in diamond," New J. Phys. **20**, 125004 (2018).
[93]L. Childress, M. V. Gurudev Dutt, J. M. Taylor, A. S. Zibrov, F. Jelezko, J. Wrachtrup, P. R. Hemmer, and M. D. Lukin, "Coherent dynamics of coupled electron and nuclear spin qubits in diamond," Science **314**, 281 (2006).
[94]J. Towns, T. Cockerill, M. Dahan, I. Foster, K. Gaither, A. Grimshaw, V. Hazlewood, S. Lathrop, D. Lifka, G. D. Peterson, R. Roskies, J. R. Scott, and N. Wilkins-Diehr, "XSEDE: Accelerating scientific discovery," Comput. Sci. Eng. **16**, 62 (2014).